Polym. Bull. (2017) 74:4453–4481
DOI 10.1007/s00289-017-1967-5

ORIGINAL PAPER

Synthesis and swelling behavior of metal-chelating superabsorbent hydrogels based on sodium alginate-*g*-poly(AMPS-*co*-AA-*co*-AM) obtained under microwave irradiation

Noor Mohammad[1] · Yomen Atassi[1] · Mohammad Tally[1]

Received: 16 October 2016 / Revised: 18 February 2017 / Accepted: 28 February 2017 /
Published online: 7 March 2017

Abstract A metal-chelating superabsorbent hydrogel based on poly(2-acrylamido-2-methylpropanesulfonic acid-*co*-acrylic acid-*co*-acrylamide) grafted onto sodium alginate backbone, NaAlg-*g*-poly(AMPS-*co*-AA-*co*-AM) is prepared under microwave irradiation. The Taguchi method is used for the optimization of synthetic parameters of the hydrogel based on water absorbency. The Taguchi L_9 (3^4) orthogonal array is chosen for experimental design. Mass concentrations of cross-linker MBA C_{MBA} initiator KPS C_{KPS}, sodium alginate C_{NaAlg} and mass ratio of monomers $C_{AM/AA/AMPS}$ are chosen as four factors. The analysis of variance of the test results indicates the following optimal conditions: 0.8 g L^{-1} of MBA, 0.9 g L^{-1} of KPS, 8 g L^{-1} of NaAlg and $R_{AM/AA/AMPS}$ equals to 1:1.1:1.1. The maximum water absorbency of the optimized final hydrogel is found to be 822 g g^{-1}. The relative thermal stability of the optimized hydrogel in comparison with sodium alginate is demonstrated via thermogravimetric analysis. The prepared hydrogel is characterized by FTIR spectroscopy and scanning electron microscopy. The influence of the environmental parameters on water absorbency such as the pH and the ionic force is also investigated. The optimized hydrogel is used as adsorbent for hazardous heavy metal ions Pb(II), Cd(II), Ni(II) and Cu(II) and their competitive adsorption is also discussed. Isotherm of adsorption and effect of pH, adsorption dosage and recyclability are investigated. The results show that the maximum adsorption capacities of lead and cadmium ions on the hydrogel are 628.93 and 456.62 mg g^{-1}, respectively. The adsorption is well described by Langmuir isotherm model. The hydrogel is also utilized for the loading of potassium nitrate as an active agrochemical agent and the release of this active agent has also been investigated.

✉ Yomen Atassi
yomen.atassi@hiast.edu.sy

[1] Laboratory of Materials Science, Department of Applied Physics, Higher Institute for Applied Science and Technology, P.O. Box 31983, Damascus, Syria

Keywords Hydrogel · 2-Acrylamido-2-methyl-1-propanesulfonic acid · Polyacrylate · Polyacrylamide · Alginate · Heavy metal removal

Introduction

Contamination of water resources by heavy metal ions has become an issue of great concern as it has adverse effects on human health [1]. These pollutants are considered metabolic poisons and enzyme inhibitors. Several techniques have been developed to remove heavy metal ions from contaminated aqueous solutions, such as coagulation and precipitation [2], electrosorption [3], ion-exchange treatment [4], membrane filtration [5], adsorption onto amino-functionalized ordered mesoporous silica [6], etc. Recently, the use of hydrogel polymers for the removal of heavy metal ions from wastewater has attracted special attention due to their ease of handling, high absorption capacity, reusability and possibility of semi-continuous operations for the treatment of contaminated effluents [7]. Hydrogels usually have well-defined three-dimensional porous structures with chemically responsive functional groups which enable them to easily captivate metal ions from wastewater and release those metal ions when the pH of the medium changes [8, 9]. The use of chelating monomers promotes hydrogel properties of heavy metal ion removal [10]. Among these chelating monomers are 2-hydroxy ethyl methacrylate (HEMA) and 2-acrylamido-2-methyl-1-propane sulfonic acid (AMPS). They are classified as two-dentate chelating vinylic monomers. The presence of electron-donor groups (Lewis bases) within polymeric network helps in binding the toxic heavy metal ions (Lewis acids) via coordination bonds and forming complex structures [10, 11]. The metal-chelating polymers are termed polychelatogens [12].

Alternatively, hydrogels based on bio-resources—carboxymethyl cellulose (CMC), sodium alginate (NaAlg), etc.—are considered as attractive bio-adsorbents since they are less expensive than the conventional adsorbents, like ion-exchange resins, zeolites or activated carbon [13, 14].

In this respect, El-Hag reported the synthesis of hydrogels composed of CMC and AMPS [15]. The prepared hydrogel showed a great capability to recover metal ions such as: Mn(II), Co(II), Cu(II), and Fe(III). Recently, Zhao et al. prepared a composite hydrogel based on AMPS and NaAlg, and studied the affinity of the hydrogel towards Cu(II) [16]. Also, Soleyman et al. reported the use of HEMA as a chelating co-monomer for synthesizing a chelating hydrogel based on salep to remove Cu(II), Pb(II), Cd(II), and Cr(III) from contaminated water [10].

In the current study, AMPS is used to enhance the heavy metal removal properties of a new multicomponent hydrogel based on NaAlg. More precisely, NaAlg is graft-copolymerized with AMPS, a partially neutralized acrylic acid (AA) and acrylamide (AM) in the presence of potassium peroxodisulfate (KPS) as an initiator and *N*,*N*′-methylene bisacrylamide (MBA) as a crosslinking agent. The co-monomers are crosslinked via microwave radiation technique [17–19]. Synthesis and swelling behavior of such copolymer gel has not been reported before. The monomers are chosen due to the following reasons: AMPS, as a hydrophilic

monomer containing nonionic and anionic moieties with strongly ionizable sulfonate groups, imparts high swellability to hydrogels at almost all pH ranges. AA and AM are anionic and nonionic monomers, respectively. They are rather cheap, common monomers for preparing superabsorbent hydrogels (SAHs). Increasing number of ionic groups (carboxylates and sulfonates) in the superabsorbents is expected to increase their swelling capacity; whereas, the nonionic groups improve the hydrogels strength and their salt tolerance. The Taguchi orthogonal experimental design is applied to optimize the operational conditions for the synthesis. The grafting is verified by FTIR. Morphological and thermal characteristics of the prepared hydrogel are investigated using scanning electron microscopy (SEM) and thermogravimetric analysis (TGA), respectively. Swelling behavior in saline and different pH media is also studied. The chelating ability of the optimized hydrogel is assessed by investigating its affinity towards different heavy metal ions Pb(II), Ni(II), Cd(II) and Cu(II). The effect of combining carboxylic and sulfonic acid groups on the metal ion retention properties of the polychelatogen is also investigated. The removal properties of the current SAH are compared with the results of other similar chelating hydrogels. Finally, potassium nitrate, as an agrochemical agent, is loaded into the hydrogel and its release in deionized water is studied.

Experimental

Chemicals and materials

NaAlg (viscosity of the aqueous solution at a concentration of 1% is 5.0–40.0 cps at 25 °C) and AMPS (for synthesis) are purchased from Sigma Aldrich. AA and AM (for synthesis) were from Merck and they are used as purchased. KPS (GR for analysis), MBA (special grade for molecular biology) and *N*,*N*,*N*′,*N*′-tetramethylene diamine (TEMED) (GR for analysis) are also obtained from Merck. Sodium hydroxide (NaOH) microgranular pure (POCH) is used for acid neutralization. Solvents methanol and ethanol (GR for analysis) are obtained from Merck. Saline solutions, sodium chloride (NaCl), magnesium chloride ($MgCl_2$) and aluminum chloride ($AlCl_3$) are prepared with distilled water and are all purchased from Merck (GR for analysis). All the metal ion reagents (Pb(II), Ni(II), Cd(II) and Cu(II)) are nitrate salts and are of analytical grade. They are purchased from Merck and used without any purification.

Experimental design

The Taguchi orthogonal experimental design was used to minimize the number of experiments and optimize the synthetic conditions for NaAlg-*g*-poly (AMPS-*co*-AA-*co*-AM). Distilled water absorbency (S_w) of NaAlg-*g*-poly(AMPS-*co*-AA-*co*-AM) was selected as the response. Based on preliminary experiments, the following factors were determined to be the most effective in the synthesis of NaAlg-*g*-poly(AMPS-*co*-AA-*co*-AM): mass concentrations of NaAlg (C_{NaAlg}),

Table 1 Various levels of each factor

Factor	Level 1	Level 2	Level 3
C_{NaAlg} (g/L): A	8	10	12
$R_{AM/AA/AMPS}$: B	1/1.4/1.7	1/2/2.8	1/1.1/1.1
C_{MBA} (g/L): C	0.8	1.0	1.2
C_{KPS} (g/L): D	0.9	1.2	1.5

Table 2 Experimental design (according to L_9 (3^4)) and the responses

Run	*A*	*B*	*C*	*D*	S_w (g g^{-1})
1	1	1	1	1	707
2	1	2	2	2	404
3	1	3	3	3	528
4	2	1	2	3	514
5	2	2	3	1	356
6	2	3	1	2	732
7	3	1	3	2	294
8	3	2	1	3	336
9	3	3	2	1	660
Mean: $\bar{S}_w$	$\bar{S}_w$ is the mean value of S_w for 9 runs in this table				503

cross-linker MBA (C_{MBA}), initiator KPS (C_{KPS}) and molar ratio of AM to AA to AMPS ($R_{AM/AA/AMPS}$).

Our preliminary laboratory trials on SAHs indicated to define three levels for each selected factor (Table 1). Thus, the Taguchi L_9 (3^4) orthogonal array was selected for experimental design. Based on the L_9 orthogonal array, 9 syntheses were conducted and each one was repeated three times. For each synthesis, mean value of the three replications was the response of this synthesis. Table 2 shows the experimental design and the corresponding responses S_w.

Preparation of NaAlg-*g*-poly(AMPS-*co*-AA-*co*-AM) superabsorbent hydrogels SAHs

The general procedure for the preparation of the superabsorbent hydrogel through graft copolymerization of poly(AMPS-*co*-AA-*co*-AM) onto NaAlg is conducted as follows.

The monomers solutions are prepared as follows: (6 g) AA is partially neutralized to 75 wt% by addition of NaOH solution (5 M) to the acid in an ice bath to avoid polymerization, then the solution is added to the solution of AM (4.25 g in ca. 9 mL of distilled water) and AMPS (7.25 in ca. 12 mL of distilled water) with continuous stirring. After that, we add the MBA solution (0.08 g in ca. 7 mL of distilled water).

NaAlg (0.8 g) is dissolved in 40 mL purified water under mechanical stirring at 60 °C for 15 min. Two equimolar aqueous solutions of the redox initiator system of

KPS, 0.09 g and TEMED, 0.038 g (each in ca. 5 mL of distilled water) are prepared and then added dropwise to the solution of NaAlg under vigorous mechanical stirring and kept at 60 °C for 10 min to generate radicals. After cooling this solution to 40 °C, the monomer solution is added dropwise on it, under continuous stirring at 1050 rpm for 15 min. The total volume of the reactive mixture is brought to 100 mL by adding distilled water. Then, the final mixture is treated in a microwave oven at the power of 950 W for 60 s. The temperature and viscosity of the mixture gradually increase and the gelation point is reached after 50 s.

The product (as an elastic yellow gel) is cut to small pieces. And it is firstly washed thoroughly with methanol several times to remove the surfactant and then is immersed 24 h in absolute methanol for dehydration and dissolving non-reacting reagent. At last, it is washed by ethanol, and dried for several hours at 60 °C until it became solid and brittle. At this point the solid is milled and treated in the furnace at 60 °C for 24 h.

Instrumental analysis

The IR spectra in the 400–4000 cm^{-1} range were recorded at room temperature on the infrared spectrophotometer (Bruker, Vector 22). For recording IR spectra, powders were mixed with KBr in the ratio 1:250 by weight to ensure uniform dispersion in the KBr pellet. The mixed powders were then pressed in a cylindrical die to obtain clean discs of approximately 1 mm thickness.

The morphology of the samples was examined using scanning electron microscope VEGA II TESCAN SEM instrument after coating the samples with graphite.

Thermogravimetric analyses of NaAlg, and the SAH were performed (SETARAM, Labsys TG, 1600 °C) from room temperature to 400 °C at a heating rate of 10 °C min^{-1} and under argon atmosphere.

A computer interface X-ray powder diffractometer (Philips, X'pert) with Cu Kα radiation ($\lambda = 0.1542$ nm) was used to identify the crystalline phases. The data collection was over the 2θ range of 10°–70° in steps of 0.02° s^{-1}.

Atomic absorption spectrophotometer (AAS) Shimadzu, AA-6800 is used to measure the adsorbance of heavy metals on the superabsorbent hydrogel.

Conductivity of prepared KNO_3 solutions is measured at room temperature by (JENWAY 4510 conductivity/TDS meter).

Swelling measurements

Water absorbency of the hydrogel is measured by the free swelling method and is calculated in grams of water per 1 g of the hydrogel. Thus, an accurately weighed quantity of the polymer under investigation (0.1 g) is immersed in 500 mL of distilled water at room temperature for at least 4 h. Then the swollen sample is filtered through weighed 100-mesh (150 μm) sieve until water ceased to drop.

The weight of the hydrogel containing absorbed water is measured after draining and the water absorbency is calculated according to the following Eq. (1):

$$S_{eq} = (w_s - w_d)/w_d, \quad (1)$$

where S_{eq} is the equilibrium water absorption calculated as grams of water per gram of superabsorbent sample; w_d and w_s are the weights of the dry sample and swollen sample, respectively [20, 21].

Gel content

In order to measure the gel content, accurately weighed dried samples of SAH NaAlg-*g*-poly(AMPS-*co*-AA-*co*-AM) are dispersed in distilled water to swell completely. Then the swollen SAHs are filtered and washed with distilled water frequently. The samples are dewatered in excess ethanol for 48 h, and dried at 50 °C for 12 h until the SAHs have a constant weight. The gel content is defined as the following equation [22]:

$$\text{Gel}\,(\%) = \frac{w_d}{w_i} \times 100, \quad (2)$$

where w_d is the weight of dried SAH after extraction and w_i is the initial weight of the SAH.

Grafting percentage and grafting efficiency

The grafting percentage ($G\%$) the grafting efficiency ($E\%$) are calculated according to Eqs. (3, 4) [23–25]:

$$G\% = \frac{w_1 - w_0}{w_0} \times 100, \quad (3)$$

$$E\% = \frac{w_1 - w_0}{w_2} \times 100, \quad (4)$$

where w_0, w_1, w_2 denote the weight of NaAlg, final weight of the grafted hydrogel and weight of monomers, respectively.

Water retention

To investigate the water retention of the hydrogel sample at constant temperature, the pre-weighed swollen gel w_3 equilibrated in distilled water is left at room temperature for 24 h. Then, the mass of the hydrogel is recorded again and marked as w_4. The percentage water retention is calculated as follows [26]:

$$\text{Water retention}\,(\%) = \frac{w_4}{w_3} \times 100. \quad (5)$$

Swelling kinetics at different pH values

To investigate the rate of absorbency of the optimized SAH at different pH values, accurately weighed quantities (0.1 g) of the optimized hydrogel NaAlg-*g*-poly(AMPS-*co*-AA-*co*-AM) are immersed in 500 mL of aqueous solutions of different pH values (pH 3.0, 7.0 and 11.0) at room temperature. At consecutive time intervals, the water absorbency of the SAH is measured according to the above-mentioned method.

Adsorption study

Pb^{2+}, Ni^{2+}, Cd^{2+} and Cu^{2+} adsorption capacities of the optimized hydrogel NaAlg-*g*-poly(AMPS-*co*-AA-*co*-AM) were also determined at ambient temperature. For each metal ion, about 0.02 g of the prepared hydrogel sample was accurately weighed into a conical flask and then 200 mL of 100 mg L^{-1} of metal ion solution (prepared from metal nitrate salt) was carefully added into the flask. The solutions were stirred at 25 °C for 4 h before it was statically placed for 24 h to allow the metal ion adsorption saturation of the NaAlg-*g*-poly(AMPS-*co*-AA-*co*-AM) sample to be achieved. Subsequently, the adsorption solution was filtered and part of the filtrate was diluted to a certain concentration for determination by an atomic absorption spectrometer. Therefore, the metal ion adsorption capacities of NaAlg-*g*-poly(AMPS-*co*-AA-*co*-AM) were calculated by Eq. (6).

$$q(\mathrm{M}^{2+}) = \frac{(c_0 - c) \times V \times M}{W}, \tag{6}$$

where $q(\mathrm{M}^{2+})$ is the divalent metal ion adsorption capacity of NaAlg-*g*-poly (AMPS-*co*-AA-*co*-AM) (mg g^{-1}), c_0 and c are the metal ion solution concentrations before and after adsorption (mmol L^{-1}), respectively. V is the solution volume (L), M is the atomic molar mass of metal ion (g mol^{-1}) and W is the mass of NaAlg-*g*-poly(AMPS-*co*-AA-*co*-AM) sample (g) [27].

As for the competitive adsorption, a solution (200 mL) containing 100 mg L^{-1} from each metal ion was treated with 0.2 g of hydrogel at 25 °C for 4 h under stirring before it was statically placed for 24 h. After adsorption equilibrium, the concentrations of metal ions in the remaining solution were also evaluated by AAS.

Loading/releasing of potassium nitrate

In this section, we study the effect of loading percentage of the optimized hydrogel with KNO_3, used as an active agrochemical agent, on the release kinetics.

0.1 g of dried hydrogel particles is immersed in 25 mL of potassium nitrate (PN) solutions with 0.5, 1, 2 wt% concentration for 24 h at room temperature. After withdrawing the loaded hydrogels, the volume of the rest solutions is filled to 25 mL and according to conductivity of these diluted solutions, the amount of loaded PN is calculated.

Loaded hydrogels are filtered and dried in an oven at 40 °C for constant weight. Then, for studying the releasing profile of PN, deionized water is chosen as releasing medium. In general, dried KNO_3-loaded hydrogels are immersed in 100 mL deionized water under un-stirred condition. The amount of PN release is evaluated using a conductimeter.

Results and discussion

Synthesis mechanism of NaAlg-*g*-poly(AMPS-*co*-AA-*co*-AM)

The hydrogels are prepared by free radical polymerization in distilled water under atmospheric condition. Graft polymerization, of AM, AA and AMPS onto NaAlg is carried out in the presence of MBA as a crosslinking agent, KPS as an initiator and TEMED as a reaction accelerator (Fig. 1). The sulfate anion radicals abstract hydrogen atoms from functional groups in NaAlg to form macroradicals. These alkoxy radicals play the role of free radical donor centers to surrounding monomers, resulting in chain initiation step. Then, free radicals on growing grafted copolymers can be coupled with the vinyl groups of MBA to form crosslinked structure.

Statistical analysis of S_w

The mean value of three replications of each S_w response is considered as the result for each run and is listed (Table 2). All statistical analysis is conducted by Minitab software (version 16). Signal-to-noise ratio (*S*/*N* ratio) is a very useful parameter to reflect the relative effects of factors since it takes both mean and variance into consideration and it is strongly suggested by Taguchi experimental design method. Larger *S*/*N* ratio indicated stronger effects of the considered factors.

S/*N* ratio is given by:

$$S/N = -10\log\left[\frac{1}{n}\sum_{i=1}^{n}\frac{1}{y_i^2}\right],$$

where y is the value of the response.

Tables 3 and 4 demonstrate the response table for means and for *S*/*N* ratios, respectively. Δ values for each factor in the two tables are given by Eq. (7) for Table 3, and Eq. (8) for Table 4, respectively:

$$\Delta_{\text{factor(mean)}} = \text{response}_{\max} - \text{response}_{\min} \tag{7}$$

$$\Delta_{\text{factor}(S/N)} = S/N_{\max} - S/N_{\min}. \tag{8}$$

The order of importance of the four factors is the same for Tables 3 and 4. The optimum levels of the factors are also the same for these two tables. Figure 2 is the main (reflected by *S*/*N* ratio) graph of each effective factor. The optimum levels of factor indicated by *S*/*N* ratios (based on Table 4 or Fig. 2) are shown in Table 5.

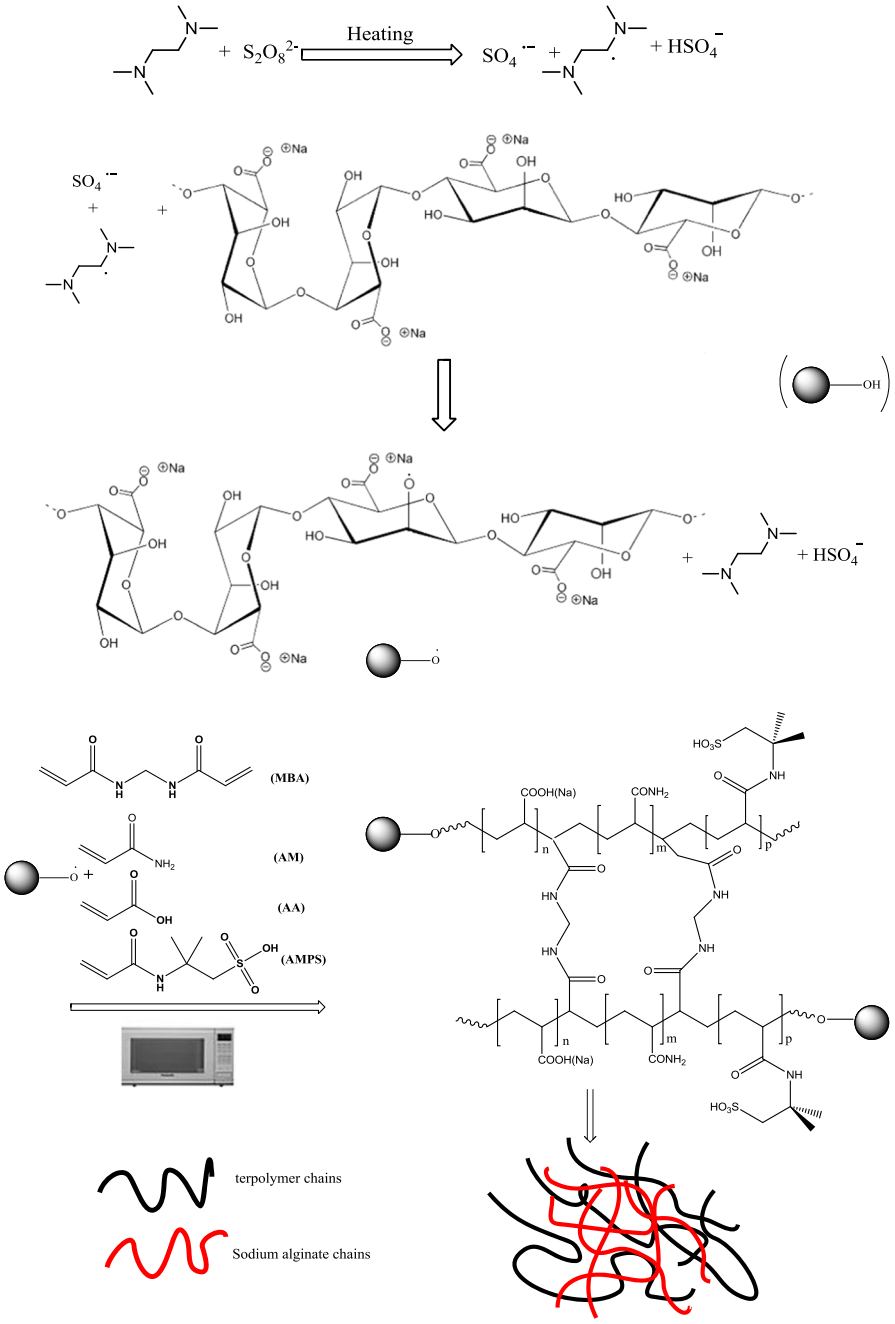

Fig. 1 Proposed reaction scheme for the synthesis of NaAlg-*g*-poly(AMPS-*co*-AA-*co*-AM) superabsorbent hydrogel

Table 3 Response table for S_w (g g^{-1}) means

Level	*A*, C_{NaAlg}	*B*, $R_{AM/AA/AMPS}$	*C*, C_{KPS}	*D*, C_{MBA}
1	546.3	505.0	574.3	591.7
2	534.0	365.3	476.7	526.0
3	430.0	640.0	459.3	392.7
Δ	116.3	274.7	115.0	199.0
Rank	3	1	4	2

Table 4 Response table for signal-to-noise ratios (for S_w); larger is better

Level	*A*, C_{NaAlg}	*B*, $R_{AM/AA/AMPS}$	*C*, C_{KPS}	*D*, C_{MBA}
1	54.52	53.52	54.80	54.94
2	54.18	51.23	52.93	54.25
3	52.09	56.04	53.07	51.62
Δ	2.43	4.82	1.87	3.32
Rank	3	1	4	2

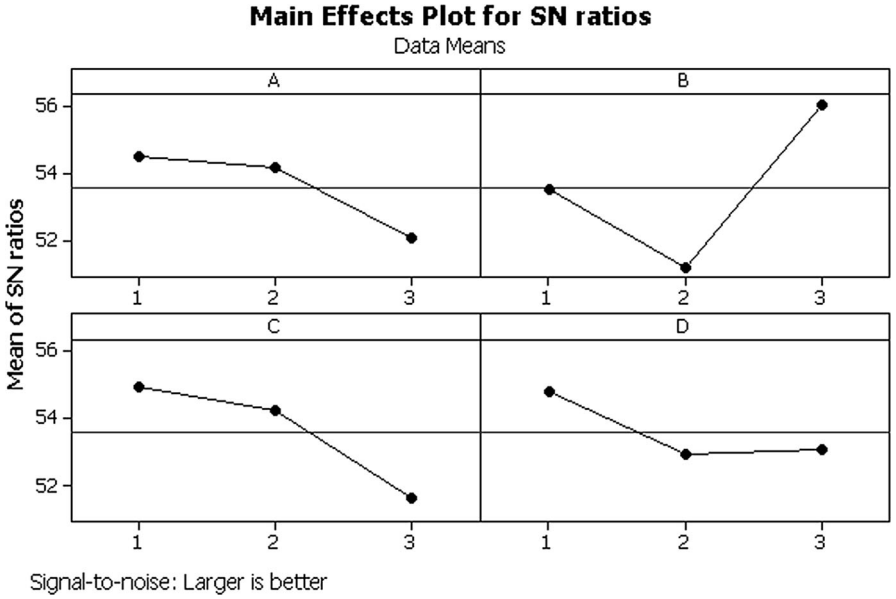

Fig. 2 Main effect (reflected by *S/N* ratio) of each factor for S_w, where *A* C_{NaAlg}, *B* $R_{AM/AA/AMPS}$, *C* C_{KPS}, *D* C_{MBA}

The optimal levels of factors indicated by mean responses (according to Table 3) are 1 (C_{NaAlg}), 3 ($R_{AM/AA/AMPS}$), 1 (C_{KPS}), 1 (C_{MBA}) and they are consistent with those given by *S/N* ratios.

Based on Taguchi method, and by taking the contribution of all factors (C_{NaAlg}, $R_{AM/AA/AMPS}$, C_{KPS}, C_{MBA}), the $S_{w(opt)}$ can be predicted as follows:

Table 5 Optimum level of each factor for S_w based on Table 4 or Fig. 2

Factor	Rank	Optimum level	Corresponding S_w (g g^{-1})
A	3	1	546
B	1	3	640
C	4	1	574
D	2	1	591

$$S_{w(opt)} = \bar{S}_w + \left[S_{w(NaAlg,1)} - \bar{S}_w\right] + \left[S_{w(AM/AA/AMPS,3)} - \bar{S}_w\right] + \left[S_{w(KPS,1)} - \bar{S}_w\right] + \left[S_{w(MBA,1)} - \bar{S}_w\right]$$

$$S_{w(opt)} = 503.4 + [546.3 - 503.4] + [640.0 - 503.4] + [574.3 - 503.4] + [591.7 - 503.4] = 842.1 \text{ g/g},$$

where $\bar{S}_w$ is the mean value of S_w for 9 runs in Table 2, $S_{w(NaAlg,1)}$, $S_{w(AM/AA/AMPS,3)}$, and $S_{w(MBA,1)}$ are the corresponding S_w means of the different factors at their optimal levels (Table 5).

Swelling results

Experiments were conducted to confirm the optimized $S_{w(opt)}$. Three replications were made to give the confirmed experimental $S_{w(exp)}$

$$S_{w(exp)} = 822 \text{ g/g}$$

The difference between the value of the optimized SAH $S_{w(opt)}$ and its corresponding experimental one is:

$$\left|S_{w(opt)} - S_{w(exp)}\right| = 842 - 822 = 20 \text{ g/g}.$$

The experimental result is very consistent with the predicted one.

FTIR spectra

In order to investigate the successful grafting of the copolymer onto NaAlg backbone, FTIR spectroscopy is employed.

Figure 3 shows the FTIR spectra of NaAlg, the copolymer poly(AMPS-*co*-AA-*co*-AM), NaAlg-*g*-P(AA-*co*-AM-*co*-AMPS), and the physical mixture of NaAlg with the copolymer.

In the spectrum of copolymer, the peaks observed at 3450 and at 3220 cm^{-1} correspond to O–H and N–H stretching, respectively. The absorbance at 2938 cm^{-1} is assigned to –C–H stretching of the acrylate group. The peaks at 1666 and at 1570 cm^{-1} are assigned to C=O stretching of the acrylamide groups and acrylate groups, respectively [17, 28]. The characteristic absorption peaks of AMPS units appear at 1042 and 1115 cm^{-1} and are attributed to symmetrical and asymmetrical stretching of S=O group.

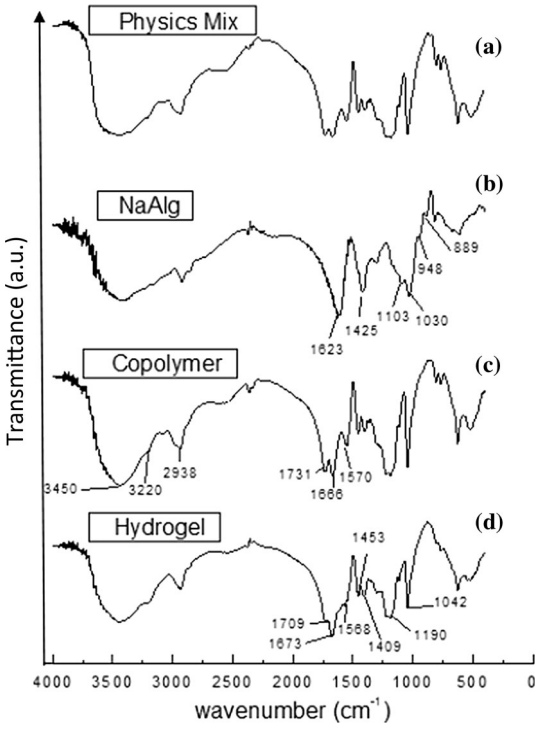

Fig. 3 FTIR spectra of *a* the physical mixture of poly(AMPS-*co*-AA-*co*-AM) with NaAlg, *b* NaAlg, *c* poly(AMPS-*co*-AA-*co*-AM) and *d* NaAlg-*g*-poly(AMPS-*co*-AA-*co*-AM)

In the spectrum of the hydrogel, the characteristic absorption bands of NaAlg at 1103 and at 1030 cm^{-1} (stretching vibration of C–OH groups) are obviously weakened after reaction, but these bands can be observed in the spectrum of the physical mixture of NaAlg and the copolymer poly(AMPS-*co*-AA-*co*-AM) with a certain intensity [29].

The absorption bands of the NaAlg spectrum at 1623 and 1425 cm^{-1} for the $–COO^-$ shift to 1568 and 1453 cm^{-1}, respectively, in the spectrum of NaAlg-*g*-poly(AMPS-*co*-AA-*co*-AM). The absorption bands at 948 and 889 cm^{-1} of NaAlg spectrum disappear in the spectrum of NaAlg-*g*-poly(AMPS-*co*-AA-*co*-AM), while appear the bands at 1190 and 1673 cm^{-1} assigned to $–COO^-$ stretching of acrylate groups and C=O stretching of acrylamide groups, respectively. This suggests the successful grafting reaction of the copolymer onto NaAlg backbone [30].

The characteristic absorption bands of NaAlg at 1623 cm^{-1} (asymmetrical stretching vibration of $–COO^-$ groups), and at 1425 cm^{-1} (symmetrical stretching of vibration of $–COO^-$ groups) are overlapped with the $–COO^-$ absorption of copolymer in this range [29].

Thermogravimetric analysis

Thermogravimetric degradation curves of the NaAlg and NaAlg-*g*-poly(AMPS-*co*-AA-*co*-AM) in argon atmosphere are displayed in Fig. 4. NaAlg thermogram

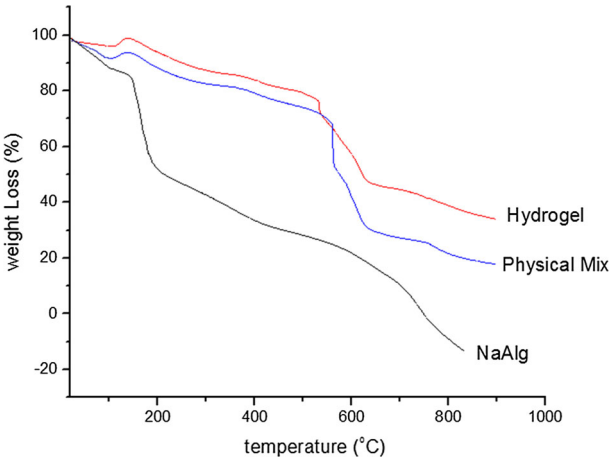

Fig. 4 TG curves of NaAlg, NaAlg-*g*-poly(AMPS-*co*-AA-*co*-AM), and the physical mixture of poly(AMPS-*co*-AA-*co*-AM) with NaAlg

exhibits two-step degradation behavior. The first one is in the range 20–145 °C, and is ascribed to the elimination of free water adsorbed to the hydrophilic polymer. The other is in the range 150–300 °C and is assigned to a complex process including dehydratation of the saccharide rings and depolymerization with the formation of water, CO_2 and CH_4 as reported in the literature [31]. The temperature of 50% weight loss is at 211.02 °C. At that temperature, the grafted hydrogel NaAlg-*g*-poly(AMPS-*co*-AA-*co*-AM) and the physical mixture exhibit weight losses of 7.1 and 12.8%, respectively.

From the TG curves, it can be concluded that the grafting of poly(AMPS-*co*-AA-*co*-AM) onto NaAlg backbone enhances the thermal stability of the polysaccharide, which suggests that the grafted hydrogel is synthesized successfully. This phenomenon has been reported Işiklan and Küçükbalcı [31]. They have indicated that grafting poly(*N*-isopropylacrylamide) onto alginate improved the thermal stability of the natural polymer.

Morphological analyses

In order to study the surface morphology of the prepared hydrogels, SEM micrographs of NaAlg-*g*-poly(AMPS-*co*-AA-*co*-AM) are performed (Fig. 5).

These micrographs verify that SAH has a porous structure. The pores are semi-open to open cells, which are connected and extend to the hydrogel inside. It is well admitted that interconnected pores and the capillary effect are responsible for improving hydrogel swelling rate [32, 33]. These pores are the regions of water permeation and interaction sites of external stimuli with the hydrophilic groups of the hydrogel [34]. ImagJ software has been used to estimate the average diameter of pores in SEM micrographs. It is about 5 μm, suggesting that SAH belongs to macroporous hydrogels [35].

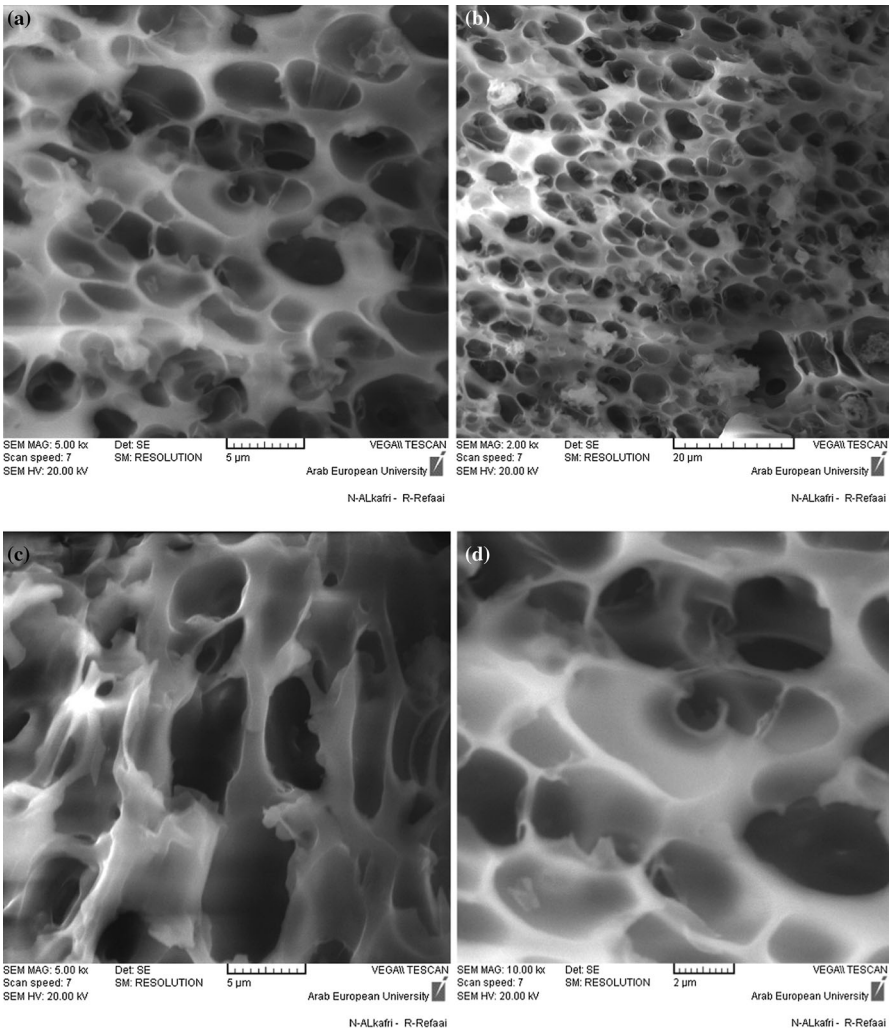

Fig. 5 SEM micrographs of the hydrogel with different magnification scales

Water retention, gel content, grafting percentage and grafting efficiency

In order to perform the functional characterization of the optimized hydrogel, water retention, gel content, grafting efficiency and grafting percentage are calculated using the procedures mentioned in the experimental section and Eqs. 2–5 (Table 6). The high values of grafting percentage, 1750.8% and grafting efficiency, 80.1% indicate the high performance of the grafting process and the successful synthesis. The high water retention capability of the hydrogel 95.3%, makes it efficient water-saving material for agricultural applications. As for the value of gel content 80%, it is comparable to gel content values recently reported by Soleyman et al. [10] 76% and by Tally et al. [27] 75%.

Table 6 Values of water retention, gel content, grafting percentage and grafting efficiency for the optimized hydrogel

Sample	Water retention (%)	Gel content (%)	Grafting percentage (*G*%)	Grafting efficiency (*E*%)
Optimized SAH	95.3	80	1750.8	80.1

Effect of particle size on water absorption and water retention

The effect of particle size on water absorption and water retention has been investigated on the optimized hydrogel NaAlg-*g*-poly(AMPS-*co*-AA-*co*-AM) (Figs. 6, 7). It can be clearly seen that the absorption capacity is diminished (about 8%) with increasing the particle size (from 180 μm to more than 425 μm), whereas water retention increases with increasing particle size. This result is linked to smaller specific surface, when particle size increases, that hinders high water absorbance capacity but promotes water retention.

Effect of the environmental parameters on water absorbency

Effects of salt solution on water absorbency

The optimized SAH was tested for the effect of water salinity on its swelling capacity.

Different concentrations of NaCl, $MgCl_2$, $AlCl_3$ solutions were prepared in order to study the effect of ion charge and ion concentration on water absorption. The absorbency of the synthesized hydrogel was measured by the same procedure adopted above in the case of distilled water.

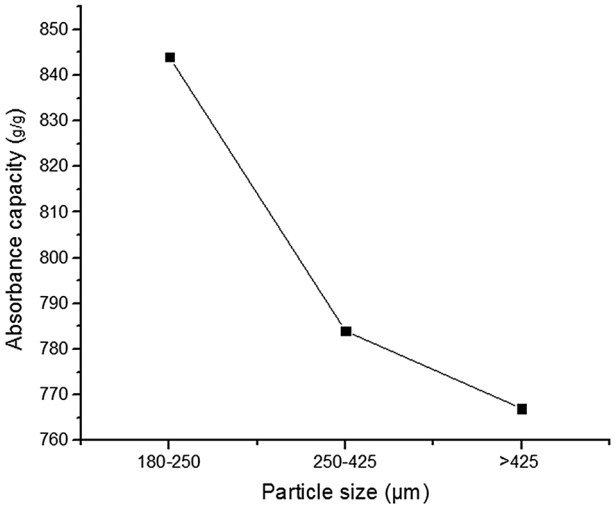

Fig. 6 Water absorption of the optimized gel with different particle size

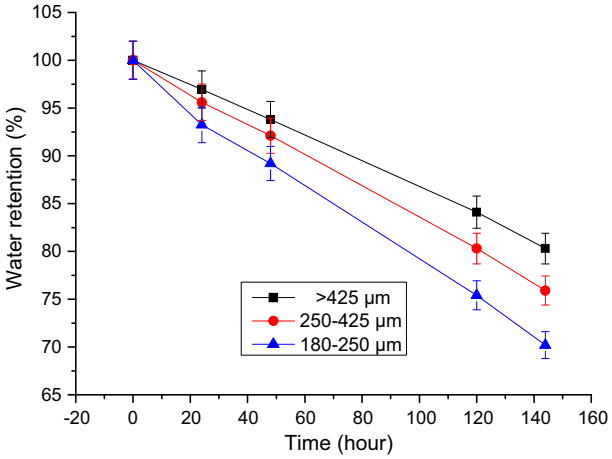

Fig. 7 Water retention of the optimized hydrogel with different particle size

Figure 8 depicts the effect of cation charge and its concentration on swelling. Since the ionic strength of a solution depends on both the concentration and the charge of each individual ion, it can be clearly seen that when the ionic strength of saline solution increases, the water absorbency decreases. This result is in agreement with the prediction of Flory equation [36]. Indeed, the presence of ions in the solution decreases the osmotic pressure difference, between the gel and the solution, which constitutes the driving force for the swelling behavior of the gel. Moreover, multivalent cations (Mg^{2+} and Al^{3+}) can neutralize several charges inside the gel by complex formation with carboxamide, carboxylate or sulfonate

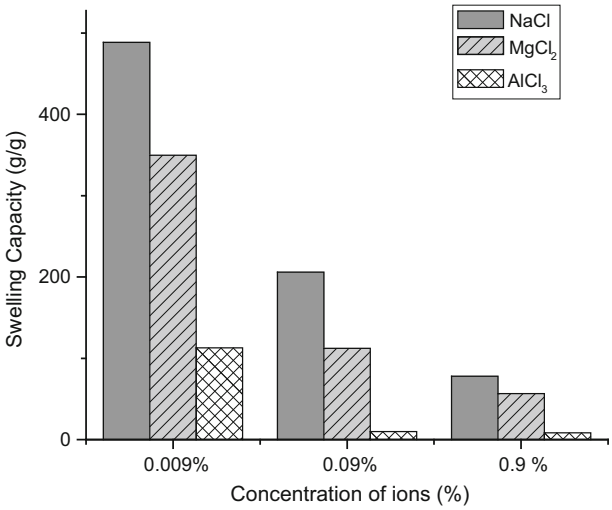

Fig. 8 Histogram of variation of water absorbency of SAH with different ion charge and ion concentration of saline solutions

groups, leading to increased ionic crosslinking degree and consequently loss of swelling.

Effect of pH on water absorbency and pH-responsive characteristics

Studies have indicated that water absorption of hydrogels are sensitive to environmental pH [37]. So, the swelling behavior of the optimized hydrogel is studied at various pH values between 2.0 and 12.0, at room temperature (Fig. 9). It is well known that the swelling capacity of all "anionic" hydrogels is highly decreased by addition of counter ions to the swelling medium. For this reason, no buffer solutions are used when studying the net effect of pH on water absorbency. Therefore, a stock of concentrated solution HCl and NaOH are diluted with distilled water to reach the desired acidic or basic pH [38].

The absorbency of the synthesized hydrogel is measured by the same procedure mentioned in the experimental section in the case of distilled water.

It can be clearly observed that the SAH slightly swells at pH 2, but it sharply swells as increasing external pH values.

As anionic polymer, the optimized SAH, contains numerous hydrophilic $–COO^-$, SO_3^- –COOH, SO_3H and NH_2 groups. At very low pH, only sulfonate groups are deprotonated, while carboxylate group on the polymer network is protonated. On one hand, the hydrogen-bonding interaction among –COOH and NH_2 groups is strengthened and the additional physical crosslinking is generated. On the other hand, the electrostatic repulsion among, $–COO^-$, SO_3^- and groups is restricted, and so the SAH network tends to shrink a little bit, and becomes slightly hydrophobic [29]. In the interval pH 4–8, some of carboxylic acid groups are ionized and the electrostatic repulsion between $–COO^-$ and SO_3^- groups causes an enhancement of the swelling capacity [17]. At high pH, the swelling capacity also decreases by

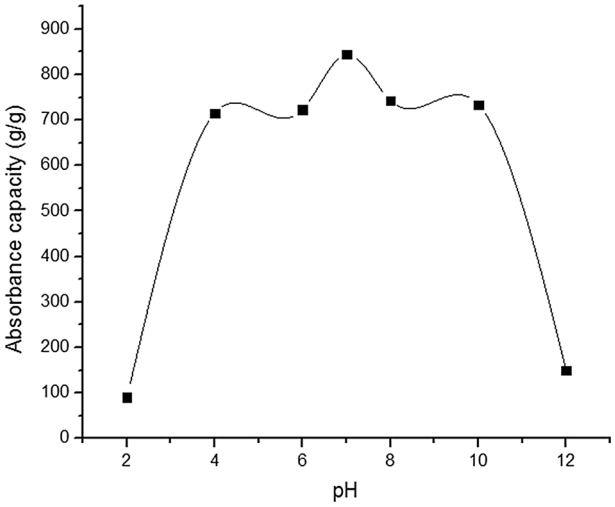

Fig. 9 Effect of environmental pH on water absorbency

"charge screening effect" of excess Na^+ in the swelling media, which shields the carboxylate anions and prevent effective anion–anion repulsion [17].

The variation of water absorption with altering the pH of external solution indicates the high pH-sensitivity behavior of the optimized hydrogel.

We have also investigated the swelling kinetics of the optimized SAH at different pH values (Fig. 10).

The effect of different pH values on the swelling kinetics is studied using Schott's pseudo-second-order swelling kinetics model [39]:

$$\frac{t}{S_w} = \frac{1}{k_{it}} + \frac{1}{S_\infty} t, \tag{9}$$

where S_w is the swelling ratio at time t, S_∞ is the theoretical equilibrium swelling ratio and k_{it} is the initial swelling rate constant.

The time-dependency of the swelling behavior of the optimized prepared hydrogel performed for different pH values is depicted in (Fig. 10). We use solutions of HCl (pH 1.0) and NaOH (pH 13.0) to adjust the pH value of the studied solution and to avoid the influence of ionic strength. The swelling kinetic parameters (k_{it} and S_∞) in various pH solutions using the Schott's pseudo-second-order kinetics model (Eq. 9) are calculated from Fig. 11. The plots of the average swelling rate (t/S_w) versus swelling time (t) give straight lines ($R^2 > 0.999$), indicating that the swelling process follows pseudo-second-order swelling kinetic model. k_{it} and S_∞ values can be calculated through the slope and intercept of the fitted straight lines. The k_{it} values for pH 3.0, 7.0 and 11.0 are 0.924, 1.634 and 1.81 g/(g s), respectively. S_∞ values are 286, 833 and 568 g g^{-1}, respectively. The S_{eq} (278, 802, 551 g g^{-1}) and S_∞ are almost equal which indicates that the swelling behavior of the SAH at different pH solutions could reach about 96% of its equilibrium absorbency within 2 h. The variation tendency of k_{it} with pH values is similar with S_∞. The initial swelling rate of the SAH is related to the relaxation rate

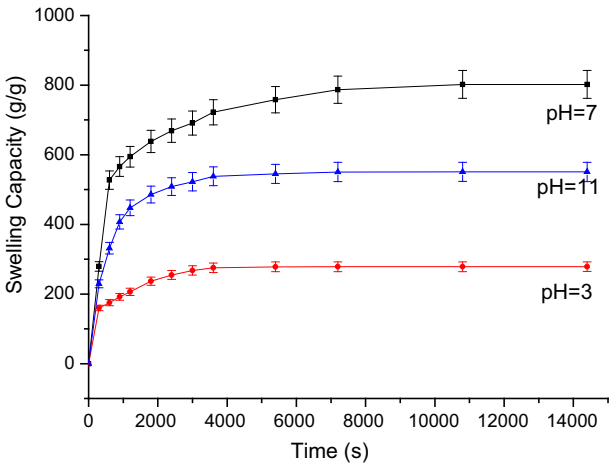

Fig. 10 Swelling kinetics at different pH values

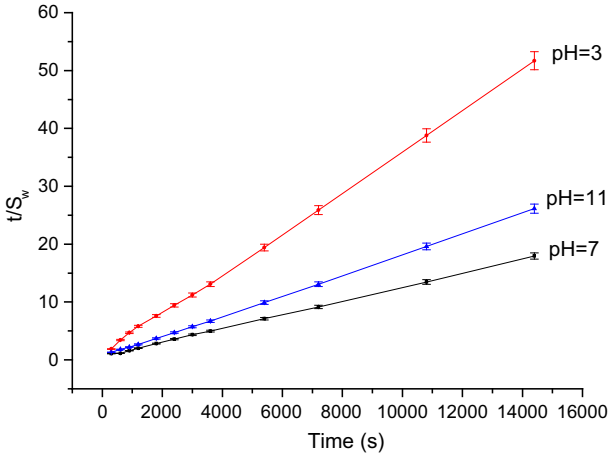

Fig. 11 Schott's pseudo-second-order swelling kinetics model for pH kinetics study

of the chain segments in the network. The ionization of carboxylate groups occurs at pH > 4.7 and this trend is increased at higher pH. On the other hand, the increased carboxylate groups lead to a stronger electrostatic repulsion, which is benefic to the relaxation of the polymer network. The fast relaxation is beneficial to the penetration of water molecules into the gel network more easily, and so the initial swelling rate can be enhanced. But at higher pH > 10, the mobility of polymer network is reduced by the screening effect of sodium cations which limits the diffusion of water molecules into the polymer network. As a result, the initial swelling rate is diminished.

Since the optimized SAH exhibits different swelling behaviors at various pH values, we investigate their pH reversibility in aqueous solutions adjusted at pH 2.0 and 7.0, respectively. Figure 12 depicts a stepwise reproducible swelling change of the SAH at 25 °C with alternating pH between 2.0 and 7.0. The time interval between the pH changes was 15 min. At pH 7.0 the hydrogel swells due to anion–anion repulsive electrostatic forces, while at pH 2.0, it shrinks within a few minutes due to protonation of carboxylate groups. This type of tests proves that the synthesized hydrogel is a smart material that responds reversibly to pH changes. The sharp swelling–deswelling behavior of the SAH makes it suitable candidate for controlled releasing systems [40].

Adsorption of heavy metal ions on the SAH

Single and multi-element aqueous solutions

Table 7 shows adsorption capacities of Pb(II), Cd(II), Ni(II) and Cu(II) on hydrogel in single and multi-element aqueous solutions.

The adsorption capacities of the optimized prepared SAH are 534.25, 258.6, 187.00 and 224.5 mg g^{-1} for Pb(II), Cd(II), Ni(II) and Cu(II), respectively. The affinity order (weight based) is Pb(II) > Cd(II) > Cu(II) > Ni(II).

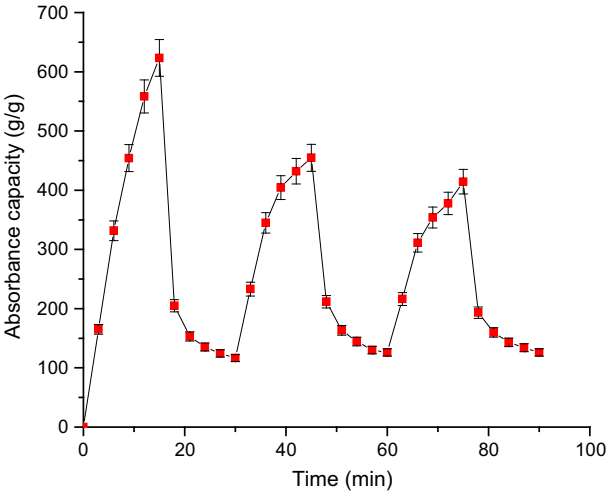

Fig. 12 Swelling–deswelling behavior of the hydrogel between pH 7.0 and 2.0, respectively. The time interval between the pH changes was 15 min

Table 7 Adsorption capacities of Pb(II), Cd(II), Ni(II) and Cu(II) on SAH (0.02 g hydrogel) in single and multi-element aqueous solutions

Metal ion	Pb(II)	Cd(II)	Ni(II)	Cu(II)
$q(M^{2+})$ (mg g^{-1})	534.25	258.6	187.00	224.5
$q(M^{2+})$ (μmol g^{-1})	2576	2297	3200	3533
$q(M^{2+})$ (mg g^{-1}) competitive adsorption	76.13	44.97	39.25	51.28
$q(M^{2+})$ (μmol g^{-1}) competitive adsorption	367	399	144	806

Since wastewater often contains more than one heavy metal species, the behavior of a particular metal specie is usually affected by the presence of other metals. So, competitive adsorption study of heavy metal ions from their mixture is also performed. The adsorption capacities decrease (Table 7). This decrease is expected due to the increased ionic strength of the aqueous solution. The affinity order (weight based) is Pb(II) > Cu(II) > Cd(II) > Ni(II).

Effect of initial heavy metal ion concentration

The effect of initial heavy ion concentration on the adsorption capacity is investigated on lead ion Pb(II) and cadmium ion Cd(II), separately as shown in Table 8. Adsorption capacity increases from 227.16 and 243.56 mg g^{-1} for 50 mg L^{-1} of initial concentration of Pb(II) and Cd(II), respectively, to 617.25 and 442.33 mg g^{-1} for 500 mg L^{-1} of initial concentration of lead ion and cadmium ion, respectively. This result is linked to a greater driving force for mass transfer of lead ion and cadmium ion from solution to solid surface at higher concentrations.

Table 8 Effect of initial heavy metal ion concentration on the adsorption capacity on optimized SAH (0.01 g hydrogel)

Metal ion Pb(II) (mg L^{-1})	50	100	200	300	500
Amount of the sorbed metal ion (Pb) (mg g^{-1})	227.16	555.28	583.04	614.59	617.25
Metal ion Cd(II) (mg L^{-1})	50	100	200	300	500
Amount of the sorbed metal (Cd) ion (mg g^{-1})	243.56	335.06	335.06	405.10	442.33

Adsorption isotherms

Langmuir and Freundlich models are usually used as isotherm models to determine the affinity of sorbent and adsorbate and to find the mechanism of adsorption. In Langmuir model, adsorption occurs as a monolayer process on homogeneous and energetically equivalent sites, while in Freundlich model, adsorption is a multilayer process and adsorbent surface is heterogeneous and energetically non-equivalent. Equations 10 and 11 express Langmuir and Freundlich isotherm models, respectively [7, 41]

$$\frac{C_{\mathrm{eq}}}{q} = \frac{1}{bQ_{\max}} + \frac{C_{\mathrm{eq}}}{Q_{\max}} \tag{10}$$

$$\log\ q = \log\ K_{\mathrm{F}} + \frac{1}{n}\log C_{\mathrm{eq}}, \tag{11}$$

where q is the concentration of the adsorbed metal ion on the adsorbent (mg g^{-1}), C_{eq} is the equilibrium metal ion concentration in solution (mg L^{-1}), b is the Langmuir constant (L mg^{-1}), and $Q_{\max}$ is the maximum adsorption capacity (mg g^{-1}), K_{F} is Freundlich constant (mg g^{-1}) and n is heterogeneity factor.

Table 9 lists the constants calculated from the plot of the two models for Pb(II) and Cd(II). As it is clearly indicated in this table, the correlation coefficients (R^2) for Langmuir isotherm model for both ions are higher than those of Freundlich model, indicating that adsorption of metal ions is better described by Langmuir isotherm model. Maximum adsorption capacities ($Q_{\max}$ (Pb) = 628.931 mg g^{-1}, $Q_{\max}$ (Cd) = 456.62 mg g^{-1}) predicted by this model are in good agreement with the values obtained experimentally 617.25 and 442.33 mg g^{-1}, respectively.

The value of free energy change (ΔG^0) for the sorption process is calculated, using Eq. (12) [41]:

$$\Delta G^0 = -RT \ln b. \tag{12}$$

The estimated values of ΔG^0 for adsorption of Pb(II) and Cd(II) onto SAH are −25.629 and −21.303kJ mol^{-1}, respectively. Negative ΔG^0 values are indicators of the spontaneous nature of the adsorption process.

The comparison of the maximum adsorption capacity of Pb(II) of the current hydrogel (628.93 mg g^{-1}) with the corresponding hydrogel prepared without AMPS (480.77 mg g^{-1}) suggests that the chelating role of AMPS promotes metal ion adsorption (Fig. 13) [27].

Table 9 Adsorption constants for the sorption of Pb(II) and Cd(II) on SAH (0.01 g optimized hydrogel)

Freundlich constants				Langmuir constants				$\Delta G°$ kJ mol^{-1}
Ion	K_F	n	R_F^2	Q_m (mg g^{-1})	b (L mg^{-1})	b (L mol^{-1})	R_L^2	
Pb(II)	174.904	3.8753	0.64587	628.93	0.14916	30,905.952	0.99875	−25.629
Cd(II)	168.873	6.1931	0.98107	456.62	0.048016	5397.479	0.99378	−21.303

Table (ii) shows adsorption capacities of some hydrogels reported in the literature (Table 10).

Soleyman et al. have recently reported the synthesis of a new chelating hydrogel via graft copolymerization of acrylamide and 2-hydroxyethyl methacrylate onto salep (a multicomponent polysaccharide) using HEMA co-monomer as a chelating hydrogel [10]. The maximum adsorption capacity of Pb(II) was 22.2 mg g^{-1}, and for Cd(II) was 21.4 mg g^{-1}. These values are to be compared with 628.93 and 456.62 mg g^{-1}, respectively, for the studied hydrogel.

Alternatively, El-Hag reported the maximum adsorption capacity of a hydrogel composed of CMC and AMPS for Cu(II) of 75.3 mg g^{-1} [15]. Zhao et al. has recently reported the maximum adsorption capacity of a hydrogel based on AMPS, acrylamide and NaAlg for Cu(II) of 75.3 mg g^{-1} [16]. Those two values are far smaller than the adsorption capacity of Cu(II) measured in the current work, 224.5 mg g^{-1}.

The enhancement of heavy metal ion adsorption capacities of the present hydrogel can be linked to the synergistic effect of sulfonates and carboxylates groups in the same structure. This was reported elsewhere in a study on a soluble polychelatogen combining carboxylic and sulfonic groups in its structure [12]. It was noticed that the metal ion retention properties of the copolymer, poly(AMPS-*co*-methacrylic acid) were enhanced with respect to both homopolymers.

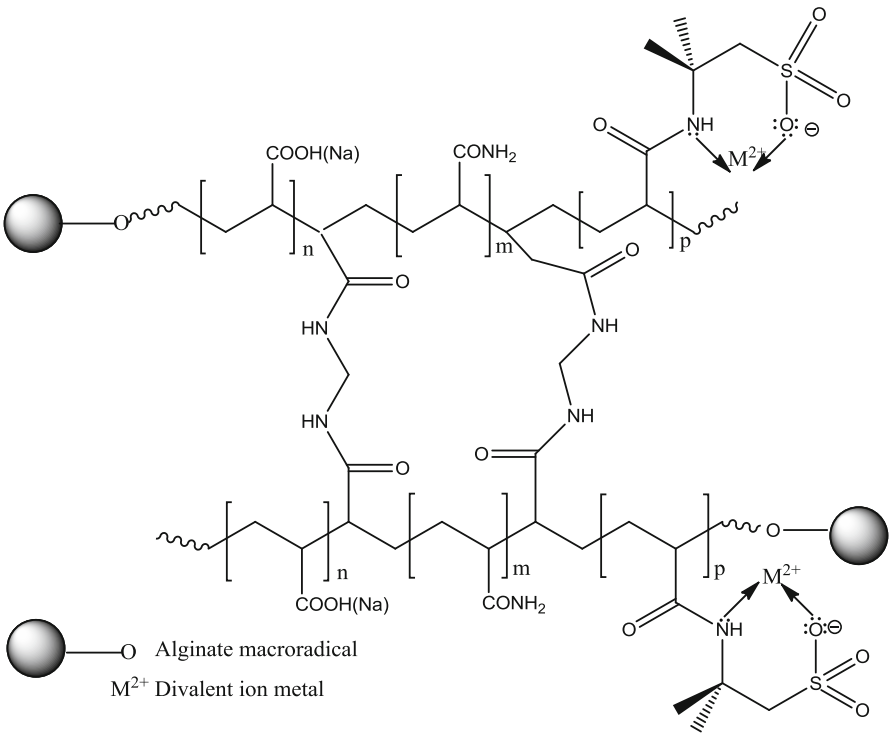

Fig. 13 Chelating role of AMPS in the hydrogel

Table 10 Adsorption capacities of some hydrogels reported in the literature

Maximum adsorption capacity (mg g^{-1})	Pb(II)	Cd(II)	Cu(II)
NaAlg-*g*-poly(AMPS-*co*-AA-*co*-AM) (current work)	628.93	456.62	224.5*
NaAlg-*g*-poly(AA-*co*-AM) [27]	480.77	–	–
Salep-*g*-poly(AM-*co*-HEMA) [10]	22.2	21.4	24.6
NaAlg-*g*-poly(AMPS-*co*-AM) [16]	–	–	46.72
CMC-*g*-poly(AMPS-*co*-AM) [15]	–	–	75.3
Bentonite/poly(AA) [7]	1666.67	416.67	222.22

* Denotes a simple adsorption capacity at initial concentration of metal ion solution 100 mg L^{-1} and 0.02 g of hydrogel

On the other hand, Bulut et al. reported the maximum adsorption capacity of Pb(II), Cd(II), and Cu(II) on a clay-based composite hydrogel, bentonite/poly(AA): 1666.67, 416.67 and 222.22 mg g^{-1}, respectively [7]. By comparing the results of the composite hydrogel with those of the current work, one can conclude that the synthesized hydrogel shows moderate absorption affinity towards lead ions, but it exhibits better absorption capacities for Cd(II) and Cu(II) ions.

In sum, the synthesized hydrogel has promising adsorption properties and it has great potential applications in protecting the environment.

Effect of initial pH

Figure 14 depicts the effect of solutions pH values on the adsorption capacity of SAH for lead ion Pb(II) and cadmium ion Cd(II). The initial concentration of Pb(II) and Cd(II) solution is 100 mg L^{-1}. The mass of SAH is about 0.02 g weighed accurately and immersed in 200 mL of pH solution. The adsorption time is set at 24 h. Figure 14 shows clearly that the adsorption capacity reaches a maximum at pH 7. In fact, when pH is $4 < pH < 8$, sulfonic acid groups and some of carboxylic acid are ionized and the electrostatic repulsions among carboxylate groups and sulfonate groups cause an enhancement of the swelling capacity. This result is in good agreement with that found when discussing the effect of environmental pH on water absorbency.

Desorption and reusability of the optimized SAH

The results above indicate that optimized hydrogel shows excellent adsorption capabilities for hazardous lead and cadmium ions. But for economic and environmental requirements, it is needed that such adsorbent material is able to be used repeatedly.

Desorption of Pb(II) and Cd(II) are achieved on samples of 0.01 g of optimized SAH loaded by different amounts of Pb(II) and Cd(II). They were stirred with HNO_3 solution—as a desorption agent—(50 mL, 0.1 M) at 25 °C for 150 min. The final metal ion concentration in the aqueous phase is determined by using AAS. The desorption ratio was calculated from Eq. (13):

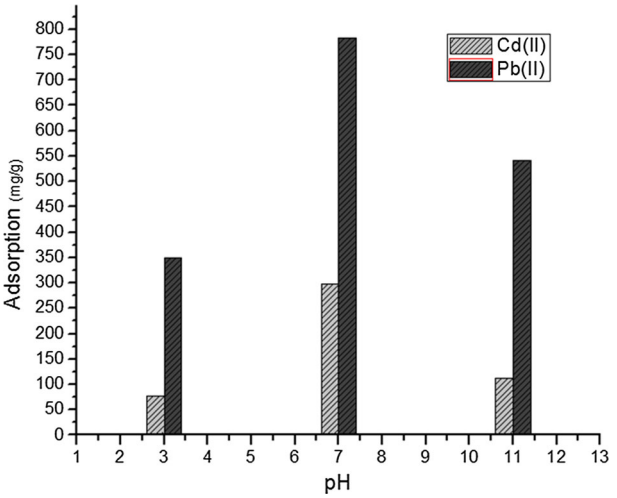

Fig. 14 Adsorption of lead and cadmium ions at different pH values on the optimized hydrogel

Table 11 Adsorption–desorption values of Pb(II) after three consecutive cycles of adsorption and desorption on SAH (0.01 g hydrogel)

Amount of Pb(II) (mg g^{-1}) loaded	208.83	555.28	583.044	614.594	866.5
Amount of the desorbed Pb(II) (mg g^{-1})	181.50	433.0	548.02	520.561	614.5
Desorption ratio (%)	87.16	77.98	93.99	84.70	70.92

Table 12 Adsorption–desorption values of Cd(II) after three consecutive cycles of adsorption and desorption on SAH (0.01 g hydrogel)

Amount of Pb(II) (mg g^{-1}) loaded	243.566	335.061	360.93	405.10	442.331
Amount of the desorbed Pb(II) (mg g^{-1})	218.641	257.5	354.74	357.0	429.5
Desorption ratio (%)	89.77	76.85	98.28	88.13	97.10

$$\text{Desorption ratio } \% = \frac{\text{amount of metal ions desorbed (mg)}}{\text{amount of metal ion adsorbed onto the SAH}} \times 100. \quad (13)$$

To determine their reusability, the desorbed hydrogels are regenerated with 0.1 mol L^{-1} NaOH for 30 min and then used for another adsorption.

The cycles of adsorption–desorption were repeated three times. Tables 11 and 12 show the adsorption–desorption values of Pb(II) and Cd(II), respectively, after three consecutive cycles of adsorption and desorption. The desorption ratios vary between 71 and 94% for Pb(II), and between 77 and 99% for Cd(II). Although the amount of ion adsorption decreases after regeneration, the hydrogel maintained nearly 83 and 90% for Pb(II) and Cd(II), respectively, of their original adsorption capacity after three consecutive cycles of adsorption and desorption. This result insinuates that the SAH is a promising candidate for the design of a continuous sorption process.

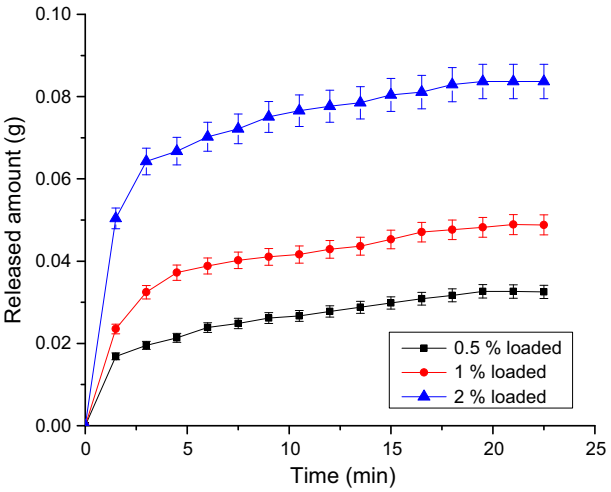

Fig. 15 PN releasing percentage from 0.5, 1, and 2% PN solutions loaded hydrogels

Loading/releasing of potassium nitrate

The results show that the loading is increased with increasing the PN concentration in loading medium (62, 146% and 269 wt% of PN loaded on hydrogel from solution containing 0.5, 1, 2 wt% of PN, respectively).

The release profile (Fig. 15) indicates that the amount of released PN increases with increasing the percentage loading of active agent. It is ascribed to the larger amount of loading. Indeed, the larger the initial load, the faster the movement of water penetrating the pores of the loaded hydrogel [42–44].

Conclusion

This work focuses the attention on the development of metal-chelating hydrogels for the assembly of new absorbents. In this study, AMPS co-monomer acts as the metal-chelating ligand. It plays the role of a two-dentate chelating co-monomer. We succeed, using microwave irradiation, to prepare this new metal-chelating hydrogel by grafting copolymer poly(AA-*co*-AM-*co*-AMPS) onto the backbone of NaAlg in the presence of a redox couple initiator KPS/TEMED and the crosslinker MBA.

The method of preparation is fast and simple. FTIR analysis confirms that the copolymer poly(AMPS-*co*-AA-*co*-AM) chains have been grafted onto the macromolecular chains of NaAlg. The Taguchi method is used to optimize the synthesis parameters. The optimized hydrogel shows a high swelling capacity (822 g g^{-1}).

The optimized hydrogel is tested for the removal of some heavy metal ions. It exhibits high adsorption capacities for Pb(II), Cd(II), Ni(II) and Cu(II) metal ions. The adsorption mechanism is better described by Langmuir isotherm model and the maximum adsorption capacities are 628.931 and 456.62 mg g^{-1} for lead and

cadmium ion, respectively. The dependence of the adsorption capacity on pH values and initial metal ion concentration is successfully evaluated. The adsorbent shows promising removal efficiency even after three cycles of adsorption/desorption. This result indicates that the optimized hydrogel is a potential cost-effective, eco-friendly and efficient adsorbing agent for hazardous heavy metal ions from wastewater. The use of the optimized hydrogel for the release of agrochemicals is successfully tested using potassium nitrate with different loading percentages.

References

1. Chen Q, Zhu L, Zhao C, Zheng J (2012) Hydrogels for removal of heavy metals from aqueous solution. J Environ Anal Toxicol S2:1–4
2. Charerntanyarak L (1999) Heavy metals removal by chemical coagulation and precipitation. Water Sci Technol 39:135–138
3. Huang SY, Fan CS, Hou CH (2014) Electro-enhanced removal of copper ions from aqueous solutions by capacitive deionization. J Hazard Mater 278:8–15
4. Dabrowski A, Hubicki Z, Podko′scielny P, Robens E (2004) Selective removal of the heavy metal ions from waters and industrial wastewaters by ion-exchange method. Chemosphere 56:91–106
5. Vijayalakshmi A, Arockiasam DL, Nagendran A, Mohan D (2008) Separation of proteins and toxic heavy metal ions from aqueous solution by CA/PC blend ultrafiltration membranes. Sep Purif Technol 62:32–38
6. Showkat AM, Zhang YP, Kim MS, Gopalan AI, Reddy KR, Lee KP (2007) Analysis of heavy metal toxic ions by adsorption onto amino-functionalized ordered mesoporous silica. Bull Kor Chem Soc 28(11):1985–1992
7. Bulut Y, Akcay G, Elma D, Serhatli E (2009) Synthesis of clay-based superabsorbent composite and its sorption capability. J Hazard Mater 171:717–723
8. Peng N, Wang Y, Ye Q, Liang L, An Y, Li Q (2016) Biocompatible cellulose-based superabsorbent hydrogels with antimicrobial activity. Carbohydr Polym 137:59–64
9. Shi Y, Xue Z, Wang X, Wang L, Wang A (2013) Removal of methylene blue from aqueous solution by sorption on lignocelluloses–g-poly(acrylic acid)/montmorillonite three-dimensional cross-linked polymeric network hydrogels. Polym Bull 70:1163–1179
10. Soleyman R, Pourjavadi A, Monfared A, Khorasani Z (2016) Novel salep-based chelating hydrogel for heavy metal removal from aqueous solutions. Polym Adv Technol 27(8):999–1005
11. Zhu Y, Zheng Y, Wang A (2015) Preparation of granular hydrogel composite by the redox couple for efficient and fast adsorption of La(III) and Ce(III). J Environ Chem Eng 3(2):1416–1425
12. Rivas B, Schiappacasse N (2003) Poly(acrylic acid-*co*-vinylsulfonic acid): synthesis, characterization, and properties as polychelatogen. J Appl Polym Sci 88:1698–1704
13. Babel S, Kurniawan TA (2003) Low-cost adsorbents for heavy metals uptake from contaminated water: a review. J Hazard Mater 97:219–243
14. Erdem E, Karapinar N, Donat R (2004) The removal of heavy metal cations by natural zeolites. J Colloid Interface Sci 280:309–314
15. El-Hag Ali A (2012) Removal of heavy metals from model wastewater by using carboxymethyl cellulose/2-acrylamido-2-methyl propane sulfonic acid hydrogels. J Appl Polym Sci 123:763–769
16. Zhao F, Qin X, Feng S (2016) Preparation of microgel/sodium alginate composite granular hydrogels and their Cu^{2+} adsorption properties. RSC Adv 6(102):100511–100518
17. Kalaleh HA, Tally M, Atassi Y (2013) Preparation of a clay based superabsorbent polymer composite of copolymer poly(acrylate-*co*-acrylamide) with bentonite via microwave radiation. Res Rev Polym 4:145–150
18. Tally M, Atassi Y (2015) Optimized Synthesis and swelling properties of a pH-sensitive semi-IPN superabsorbent polymer based on sodium alginate-*g*-poly(acrylic acid-*co*-acrylamide) and polyvinylpyrrolidone and obtained via microwave irradiation. J Polym Res 22(9):1–13

19. Kalaleh HA, Tally M, Atassi Y (2015) Optimization of the preparation of bentonite-*g*-poly(acrylate-*co*-acrylamide) superabsorbent polymer composite for agricultural applications. Polym Sci Ser B 57(6):750–758
20. Zohuriaan-Mehr MJ, Kabiri K (2008) Superabsorbent polymers materials: a review. Iran Polym J 17:451–477
21. El-Sayed M, Sorour M, AbdElMoneem N, Talaat H, Shalaan H, ElMarsafy S (2011) Synthesis and properties of natural polymers-grafted-acrylamide. World Appl Sci J 13:360–368
22. Ghasemzadeh H, Ghanaat F (2014) Antimicrobial alginate/PVA silver nanocomposite hydrogel, synthesis and characterization. J Polym Res 21:355–368
23. Jeng YT (2015) Preparation and characterization of controlled release fertilizers using alginate-based superabsorbent polymer for plantations in Malaysia. Master thesis, University Tunku Abdul Rahman, Malaysia
24. Rashidzadeh A, Olad A, Salari D, Reyhanitabar A (2014) On the preparation and swelling properties of hydrogel nanocomposite based on sodium alginate-*g*-poly(acrylic acid-*co*-acrylamide)/clinoptilolite and its application as slow release fertilizer. J Polym Res 21:344–359
25. Huang M, Shen X, Sheng Y, Fang Y (2005) Study of graft copolymerization of *N*-maleamic acid-chitosan and butyl acrylate by γ-ray irradiation. Int J Biol Macromol 36:98–102
26. Bao Y, Ma J, Li N (2011) Synthesis and swelling behaviors of sodium carboxymethyl cellulose-*g*-poly(AA-*co*-AM-*co*-AMPS)/MMT superabsorbent hydrogel. Carbohydr Polym 84:76–82
27. Tally M, Atassi Y (2016) Synthesis and characterization of pH-sensitive superabsorbent hydrogels based on sodium alginate-*g*-poly(acrylic acid-*co*-acrylamide) obtained via an anionic surfactant micelle templating under microwave irradiation. Polym Bull 22(9):1–26
28. Spagnol C, Rodrigues FHA, Neto AGVC, Pereira AGB, Fajardo AR, Radovanovic E, Rubira AF, Muniz EC (2012) Nanocomposites based on poly (acrylamide-*co*-acrylate) and cellulose nanowhiskers. Eur Polym J 48:454–463
29. Wang W, Wang A (2010) Synthesis and swelling properties of pH-sensitive semi-IPN superabsorbent hydrogels based on sodium alginate-*g*-poly(sodium acrylate) and polyvinylpyrrolidone. Carbohydr Polym 80:1028–1036
30. Hua S, Wang A (2009) Synthesis, characterization and swelling behaviors of sodium alginate-*g*-poly(acrylic acid)/sodium humate superabsorbent. Carbohydr Polym 75:79–84
31. Işiklan N, Küçükbalcı G (2012) Microwave-induced synthesis of alginate-graft-poly(*N*-isopropylacrylamide) and drug release properties of dual pH- and temperature-responsive beads. Eur J Pharmacol Biopharm 82:316–331
32. Lim DW, Yoon KJ, Ko SW (2000) Synthesis of AA-based superabsorbent interpenetrated with sodium PVA sulfate. J Appl Polym Sci 78(14):2525–2532
33. Poorna KSVC, Singh A, Rathore A, Kumar A (2016) Novel cross linked guar gum-*g*-poly(acrylate) porous superabsorbent hydrogels: characterization and swelling behaviour in different environments. Carbohydr Polym 149:175–185
34. Pourjavadi A, Amini-Fazl MS, Ayyari M (2007) Optimization of synthetic conditions CMC-*g*-poly (acrylic acid)/Celite composite superabsorbent by Taguchi method and determination of its absorbency under load. Express Polym Lett 1(8):488–494
35. Ganji F, Vasheghani-Farahani S, Vasheghani-Farahani E (2010) Theoretical description of hydrogel swelling: a review. Iran Polym J 19(5):375–398
36. Lanthong P, Kiatkamjornwong S (2006) Graft copolymerization, characterization, and degradation of cassava starch-*g*-acrylamide/itaconic acid superabsorbents. Carbodydr Polym 66:229–245
37. Gils PS, Ray D, Mohanta GP, Manavalan R, Sahoo PK (2009) Designing of new acrylic based macroporous superabsorbent polymer hydrogel and its suitability for drug delivery. Int J Pharm Pharm Sci 1:43–54
38. Hosseinzadeh H, Sadeghzadeh M, Badazadeh M (2011) Preparation and properties of carrageenan-*g*-poly(acrylic acid)/bentonite superabsorbent composite. J Boimater Nanobiotechnol 2:311–317
39. Schott H (1992) Swelling kinetics of polymers. J Macromol Sci B 31:1–9
40. Ashraf MU, Hussain MA, Muhammad G, Haseeb MT, Bashir S, Hussain SZ, Hussain I (2017) A superporous and superabsorbent glucuronoxylan hydrogel from quince (*Cydonia oblanga*): stimuli responsive swelling, on-off switching and drug release. Int J Biol Macromol 95:138–144
41. Bulut Y, Gözübenli N, Aydin H (2007) Equilibrium and kinetics studies for adsorption of direct blue 71 from aqueous solution by wheat shells. J Hazard Mater 144:300–306

42. Mahdavinia GR, Mousavi SB, Karimi F, Marandi GB, Garabaghi H, Shahabvand S (2009) synthesis of porous poly (acrylamide) hydrogels using calcium carbonate and its application for slow release of potassium nitrate. Express Polym Lett 3:279–285
43. Kim SW, Bae YH, Okano T (1992) Hydrogels: swelling, drug loading, and release. Pharm Res 9:283–290
44. Bajpai AK, Giri A (2002) Swelling dynamics of a macromolecular hydrophilic network and evaluation of its potential for controlled release of agrochemicals. React Funct Polym 53(2):125–141